



LABORATORI NAZIONALI DI FRASCATI
SIS-Pubblicazioni

LNF-04/24(P)
15 November 2004

A scintillating-fiber beam profile monitor for the DAFNE BTF

M. Anelli, B. Buonomo, G. Mazzitelli and P. Valente
Laboratori Nazionali di Frascati dell'INFN, Frascati, Italy.

Abstract

A scintillating-fiber beam profile detector has been designed, built and tested, for the monitoring of the position and size of the electron beam of the DAΦNE BTF, the recently commissioned electron beam-test facility at the Frascati LNF. A description of the detector construction and assembly, together with the results achieved during the 2003-2004 runs, are here reported.

PACS: 29.40.Mc, 41.85.Ew, 41.75.Fr

Keywords: Scintillating fiber; Beam profile; Electron and positron beam

1 Introduction

The DAΦNE Beam-test facility (BTF) provides electron/positron beams with a well-defined number of particles in a wide range of multiplicity and energy, mainly for detector calibration purposes. It was commissioned in 2002 and it has delivered beam to user experiments during all years 2003-2004 [1,2].

A number of detectors have been used for the beam diagnostics during the commissioning phase and during the users running periods; these detectors were mainly intended for the measurement of the number of particles in the beam, in the full operational range of energy, between 25 and 750 MeV, and multiplicity, from single particle to 10^{10} particles/bunch.

However, a very important point for the operation of the facility is the measurement of the beam spot position and size, in all the different multiplicity and energy configurations and with non-destructive detectors. High-fluorescence metallic flags are not sensitive at very low beam intensities down to the single electron mode, so that position sensitive particle detectors should be used.

For this purpose, a scintillating-fiber detector has been designed, built and tested during the years 2003-2004 BTF running period. The detector is described in Sec. 2 together with some details on the construction and on the readout and acquisition system, while some experimental results with the BTF electron/positron beam are reported in Sec. 3.

2 Detector design and construction

2.1 Design considerations

Taking into account cladded scintillating fibers, such as Pol.Hi.Tech type 0046, a light yield of 3-4 photoelectrons/mm (pe) at 0.5 m photocathode distance has been measured in the past [3]. The light yield depends on the quantum efficiency of the photomultiplier and on the quality of the optical coupling with the fibers. In order to have a few pe per incident particle even without optimal coupling to the photocathode (e.g. without employing optical grease), a few layers of fibers have to be stacked one over the other. This should give a sufficient light yield already with only one electron crossing the detector. Moreover, by properly staggering the layers, a multi-layer detector allows to minimize dead spaces between the fibers.

Considering a 4 layers detector of 1 mm fibers, a light yield of 1-2 pe/particle at the photocathode can be conservatively estimated. For a typical photomultiplier gain in the range 10^6 - 10^7 a charge signal of 0.1-1 pC/particle can then be estimated; this should allow both to be sensitive to single electrons, and to reach the 100-1000 particles/bunch range without saturation, for a typical 12-bit, 0.25 pC/count, charge integrating ADC.

For a given size of the detector, the number and the area of photocathodes determines the the number of readout channels and the number of fibers to be bundled together. Since the typical BTF beam spot has a Gaussian distribution with $\sigma_x \simeq \sigma_y \simeq 5$ mm, a two-view detector should have a size of at least 5×5 cm², and a millimetric spatial resolution.

A detector consisting of two planes of four layers of 48 fibers of 1 mm diameter with a readout pitch of 3 mm, will need only 32 channels, and should still be capable of a millimetric spatial resolution. A total depth of 8 mm of scintillating fibers corresponds to $\approx 0.02X_0$, thus giving an almost negligible effect on the beam energy and spot.

2.2 Scintillating fibers

A two view detector has been constructed, consisting of two identical modules to be mounted with the fibers running at 90°. A single module consists of four layers of 1 mm diameter cladded scintillating fibers, Pol.Hi.Tech type 0046. The 1 m long fibers have been cut in two ~ 50 cm pieces, then four stacked layers of 48 fibers glued side-by-side have been assembled, staggered by 0.5 mm, as shown in the scheme of Fig. 1.

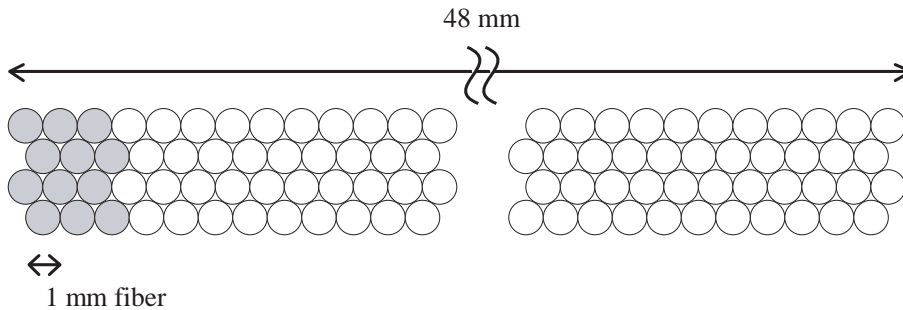


Figure 1: Scheme of the scintillating fibers detector layout: four layers of 48 fibers are stacked together (with a 0.5 mm stagger).

The fibers have been glued together by means of optical glue, the BICRON

BC600 Optical Cement, a two component¹ clear epoxy resin specifically developed for optical joints with plastic scintillators. A photograph of the first layer of 48 scintillating fibers glued together is shown in Fig. 2; the typical hardening time for each glued layer was 48 hours.



Figure 2: Gluing one layer of 48 scintillating fibers.

In Fig. 3 a photograph of the four layers of scintillating fibers are shown after the gluing, and before wrapping them in a thin foil of aluminum. In the same photograph the photomultiplier used for the readout is also shown (see in the following).

2.3 Multi-anode photomultiplier

We have chosen the Hamamatsu H6568 multi-anode photomultiplier (MAPMT) metal package, based on the R5900-00-M16 tube with a photocathode segmented in 16 pixel of $4.2 \times 4.2 \text{ mm}^2$ each; the package also includes the voltage divider circuit. This MAPMT has a good gain uniformity, low crosstalk with neighboring channels (below 1%) and good timing performances (1 ns rise time, 0.3 ns FWHM transit time spread).

We usually set the high voltage to -750 V, corresponding to a gain of $\approx 2 \times 10^6$.

¹We have mixed 100 parts by weight of resin and 28 parts by weight of hardener.



Figure 3: The four layers of scintillating fibers after the gluing (on the right), showed together with the multi-anode PMT (on the left).

A group of three fibers for each of the four layers have been bundled together to cover the area of a MAPMT pixel (such a group of 12 fibers is represented by the shaded circles in the schematic view of Fig. 1).

2.4 Detector assembly

For each of the two detector planes, the 16 bundles, constituted by 12 scintillating fibers, have been inserted in a grooved PVC mask, fitting the dimensions of the photomultiplier package ($\sim 30 \times 30 \text{ mm}^2$), in order to couple each bundle to a pixel on the MAPMT surface. Since the area of a single pixel is of $4.2 \times 4.2 \text{ mm}^2$, the PVC mask should have been grooved with $\approx 4 \text{ mm}$ side square holes, in order to fit all the fibers in a bundle. However, for sake of construction simplicity and mechanical robustness, the mask has been grooved with 4 mm diameter *circular* holes, so that only 11 out of 12 fibers per bundle are actually coupled to each MAPMT pixel. This is not a problem, both from the point of view of the uniformity and of the total yield of light.

A drawing of the mask is shown in Fig. 4, while in Fig. 5 a photograph of the PVC mask with the 16 scintillating fibers bundles, inserted and ready to be coupled to the MAPMT, is shown.

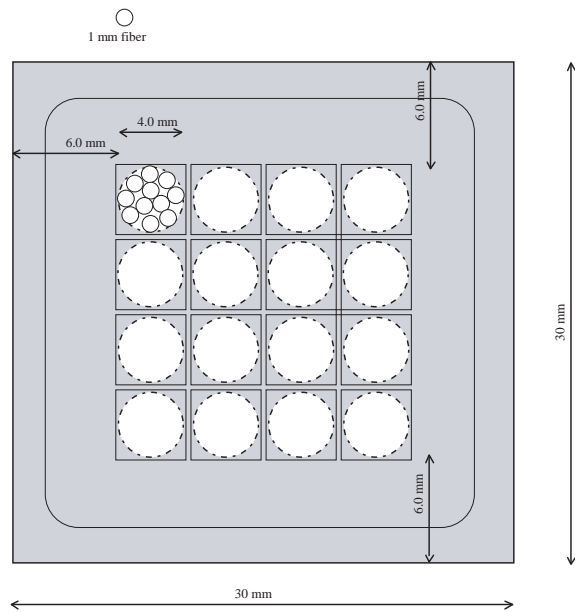


Figure 4: Drawing of the mask for the scintillating fibers bundles, for the coupling to the photocathode surface. For this 4×48 scintillating fibers detector the 16 bundles consist of 12 fibers. The fibers fit a ≈ 4 mm side square, while only 11 fit a 4 diameter circle. For sake of construction simplicity, a PVC mask with circular holes has been realized, so that only 11/12 fibers per bundle are coupled to each MAPMT pixel.



Figure 5: The PVC mask with the 16 scintillating fibers bundles inserted and ready to be coupled to the Hamamatsu H6568 MAPMT.

The two planes of the detector have been then wrapped in aluminum foils, as shown in Fig. 6, and finally they have been mounted at 90° , by means of a mechanical support as shown in Fig. 7.

2.5 Layout on the beam

During the first test runs, only one plane of the detector was installed, at the BTF beam exit (at 45°) usually dedicated to the user setups, just before the AIRFLY fluorescence chamber, with the fibers running in the vertical direction, for measuring the x profile.

In all the following BTF running periods, both the x and y views of the detector were mounted, on their mechanical support, again, right at the exit of the BTF beam for the users (Fig. 8).

2.6 Detector readout

The 16 analog signals of the MAPMT pixels are splitted in two by a passive splitter board. The suitably delayed signals are digitized by a CAEN V792 charge integrating ADC, 0.25 pC/count. The gate signal, 100 ns long, is generated starting from a reference signal generated by the LINAC timing



Figure 6: The fiber detector being wrapped with an aluminum foil.

circuit for each beam pulse. The analog signals are also digitized by means of a low threshold discriminator (CAEN V814), with a typical threshold of $35 \text{ mV}/50\Omega$, and the time of each channel is measured by means of a CAEN V775 VME TDC, $35 \text{ ps}/\text{count}$. The VME controller, a VMIC 7740 Pentium III CPU with Tundra VME-PCI chip, runs Red Hat Linux 7.2 and a LabVIEW 6.1 DAQ program. Further details on the DAQ can be found in Ref. [1].

3 Experimental results

The beam profile is measured starting from the pulse height measured in each of the 2×16 MAPMT pixels, by means of the charge integrating ADC (once having subtracted the pedestal). This pulse height infact should be proportional to the charge deposited in each fibers bundle.

Since the detector is very thin, $\approx 2\%$ of a radiation length, each electron transversing it should have a well defined average energy loss, of course with fluctuations following the typical Landau distribution, so that the average charge in a pixel should be proportional to the total number of electrons

Figure 7: The two views of the fiber detector assembled together with the fibers running horizontally (y view) and vertically (x view) in the plane perpendicular to the beam direction.

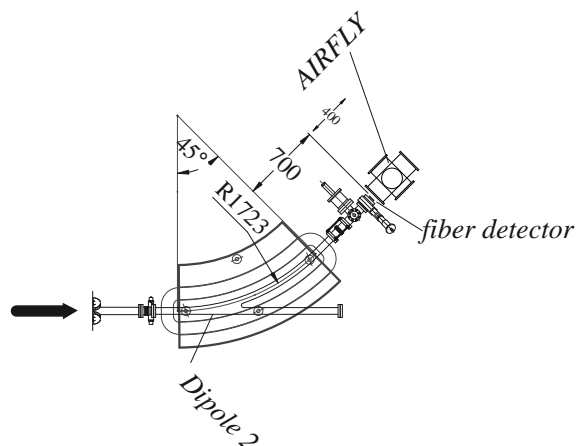


Figure 8: The scintillating fiber detector is usually placed at the the 45° beam exit (with the final dipole on), dedicated to user setups.

crossing the corresponding bundle.

In order to check this, the pulse height in the fiber detector has been measured in a run at low electron multiplicity, i.e. in single electron mode. Since the number of particles in the beam follows the Poisson statistics, the pulse height in the calorimeter, placed downstream of the fiber detector, has been used to separate events with none, one or two electrons crossing the detector.

In Fig. 9 the pulse height in one view of the detector, summed over all the fibers, is shown as a function of the pulse height in the calorimeter, for a run at 493 MeV, with an average multiplicity of 1 particle/pulse. Using the total energy deposited in the calorimeter, placed \approx a 1.5 m distance from the beam exit window, at a distance of 1.1 m from the fiber detector, one can separate one and two electrons events, the pulse height spectrum in the fibers clearly follows a Landau distribution.

The shape and the position of the beam spot can then be determined by the charge-weighted distribution of events in the 16 “fingers”, 3 mm wide, of fibers constituting each of the two views of the detector. Since the BTF is usually operated at the maximum repetition rate of 49 bunches/s, an accurate measurement of the beam spot can be achieved already accumulating a few seconds of beam, even at the lowest particle multiplicity, i.e. in single electron mode.

A possible problem in building the charge-weighted distribution can be the non-uniformity of the response of each “finger”, when crossed by a single electron. This can be due to a number of reasons; the main one in our

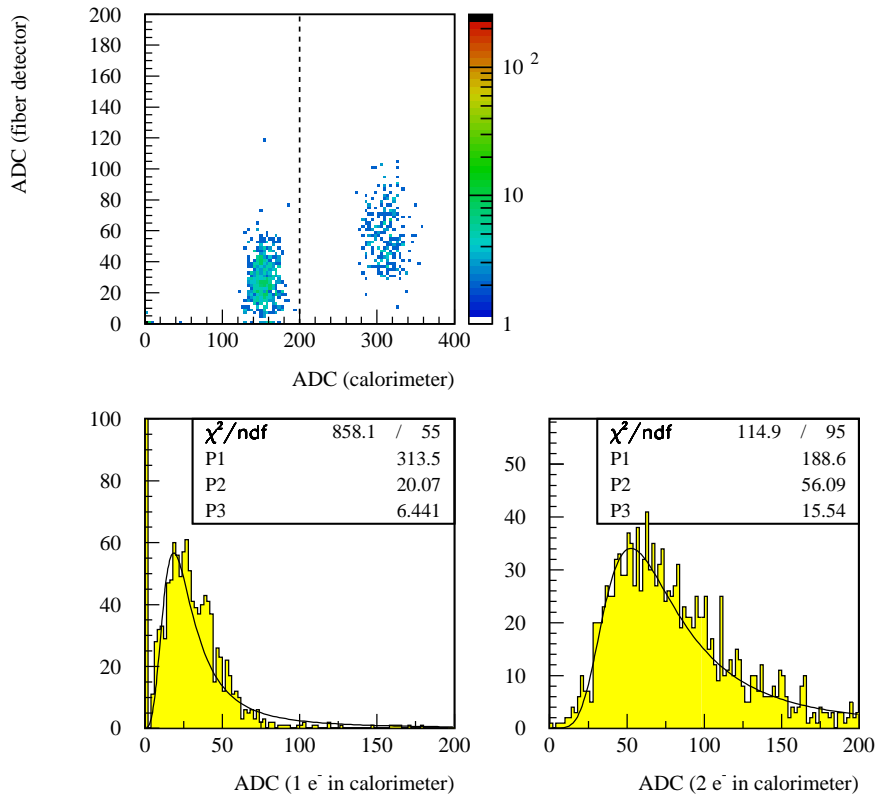


Figure 9: Top: correlation of the pulse height in the fiber detector (sum of the 16 MAPMT channels pedestal subtracted) with the pulse height in the calorimeter (see text). Bottom: the fiber detector pulse height spectrum for events with one (left plot) or two electrons (right plot), fits to the Landau function are also shown.

case is the non-optimal coupling of the fiber bundles to the surface of the MAPMT cathode, since no optical glue has been used, and to the possibility of breaking one or more fibers when inserting the bundles in the grooved PVC mask.

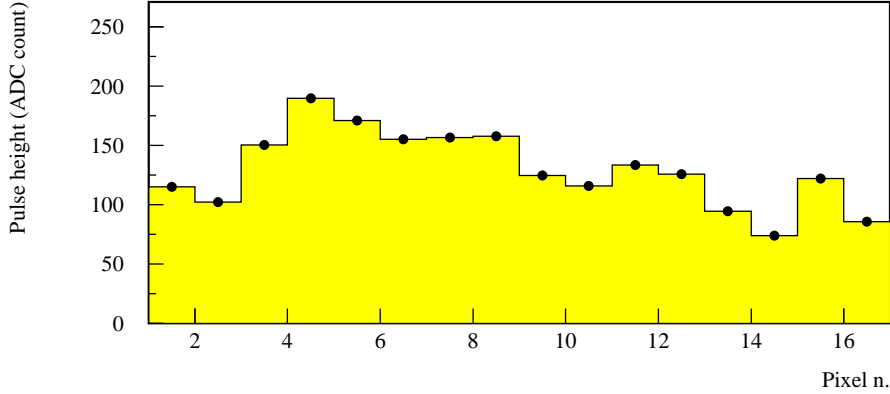


Figure 10: Pulse height of the 16 MAPMT channels (pedestal subtracted); in order to have an approximately uniform illumination (the detector was arranged with the fibers running in the horizontal direction, with the beam defocussed in the vertical plane). This spectrum has been used for the pixel equalization; the yield differences between the pixels are mainly due to broken/inefficient fibers (as shown by the groups of pixels with approximately the same yield).

In order to estimate the uniformity of response of the pixels in each view of the detector, dedicated runs with intermediate multiplicity and a very defocussed beam have been analyzed. In this data, the beam is constituted by a few tens of electrons distributed over an area, at the beam exit window, of $\approx 55 \times 25 \text{ mm}^2$, so that the surface of the fiber detector is almost uniformly illuminated. In this condition we could expect an uniform response from all the 16 channels in one view. In Fig. 10 the pulse height distribution (pedestal subtracted) of all the channels of one view is shown. There are evident yield differences between the pixels; since there are anyhow groups of pixel with approximately the same response, the differences can mainly be interpreted as due to broken or inefficient fibers in the single bundles.

The normalized output in the defocussed beam conditions are used to correct the relative yield of each pixel, for both views of the detector.

In order to check the functionality of the first of the two detector planes, some runs were taken moving the beam along the horizontal axis (with the detector arranged with the fibers running along the vertical axis), using a

standard focussed beam setting of the BTF, yielding 493 MeV electrons, on average 1 electron per pulse, with a spot size of few mm. The horizontal position of the beam has been changed by changing the current of the last bending magnet in small steps (2 A on a nominal setting of 335A), thus resulting in a nominal deviation of ≈ 7 mm at the beam exit window. The results of this scan in the horizontal direction are shown in Fig. 11.

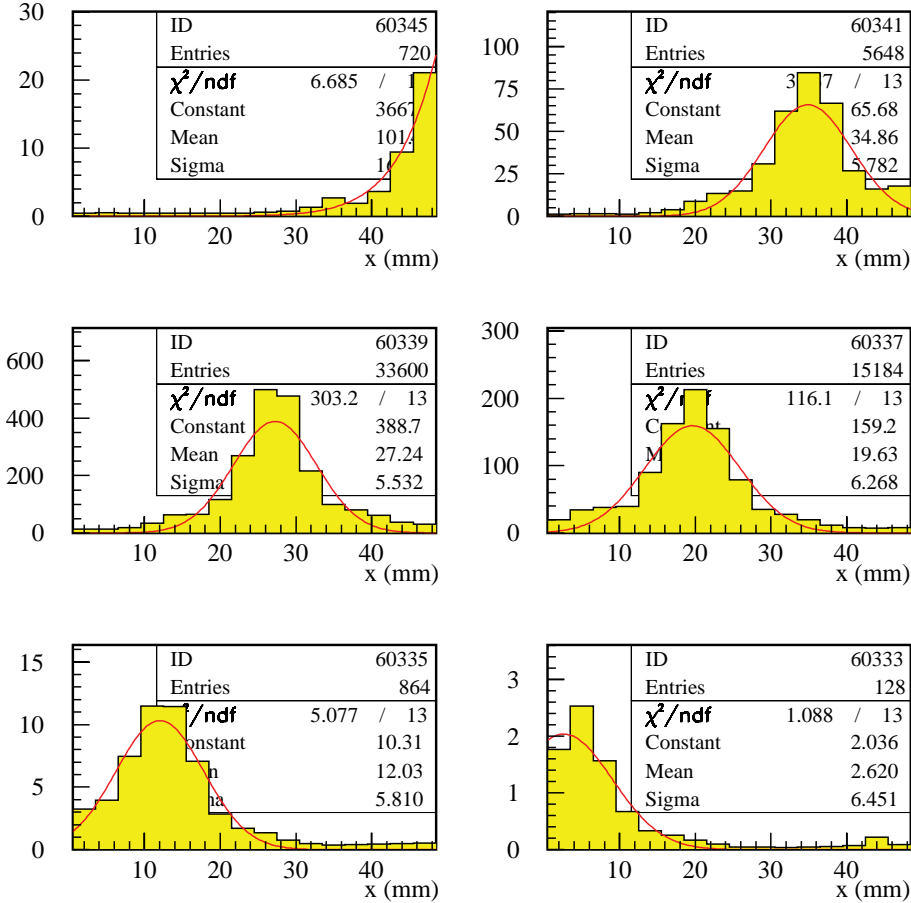


Figure 11: Charge-weighted profile for six different settings of the final bending, corresponding to a scan in the horizontal direction (along the x axis).

The shape of the charge-weighted profile is well reproduced by a Gaussian. By fitting the distribution, the mean values well reproduce the expected beam deviation. Concerning the width of the distribution, different contribution can be identified:

- the intrinsic beam spot size; this has been measured with much more accurate detectors (AGILE Silicon Tracker) to be fairly Gaussian with

$\sigma \simeq 2.2$ mm in both dimensions (with the optimized focussed beam setting we were using, of 493 MeV single electron beam); this includes the natural width of the beam plus the multiple scattering contribution on the thin aluminum exit window;

- the resolution of the fiber detector;
- if the detector is placed at some distance from the exit window, the contribution of the multiple scattering in air.

Since the multiple scattering is momentum-dependant, this contribution can be disentangled by performing the beam spot measurement at different beam energies; of course this is possible only if the beam spot size is not significantly changed by changing the BTF line settings for the different momentum settings.

The measured beam profiles, only for the horizontal view of the fiber detector, in a wide range of electron energy, with an optimal focussing of the beam and with horizontal collimators almost completely closed (thus with an approximately unchanged intrinsic horizontal beam size), are shown in Fig. 12.

The σ values for the Gaussian fits of the profiles of Fig. 12 are shown in Fig. 13 as a function of the beam energy. The expected $1/(\beta cp)$ dependance for the multiple scattering contribution can be observed at low energies, while the measured beam spot approaches a constant value at energies above 400 MeV, of ≈ 3 mm. Two main effects contribute to the plateau value: the spatial resolution of the fiber detector and the widening of the beam spot due to the intrinsic divergence, that is not negligible even if the beam is strongly collimated in the BTF line.

Another important point is the possibility of using the fiber detector also at intermediate beam intensities, i.e. between tens and thousands of particles per pulse, without any significant performance loss. In order to check this, the beam spot has been monitored for a focussed beam while increasing the beam intensity. No significant difference in the measured beam spot can be found up to several hundreds particles per bunch, as shown in the example in Fig. 14, where the horizontal profile is shown for a single particle beam, for ≈ 150 , up to more than 600 particles/pulse.

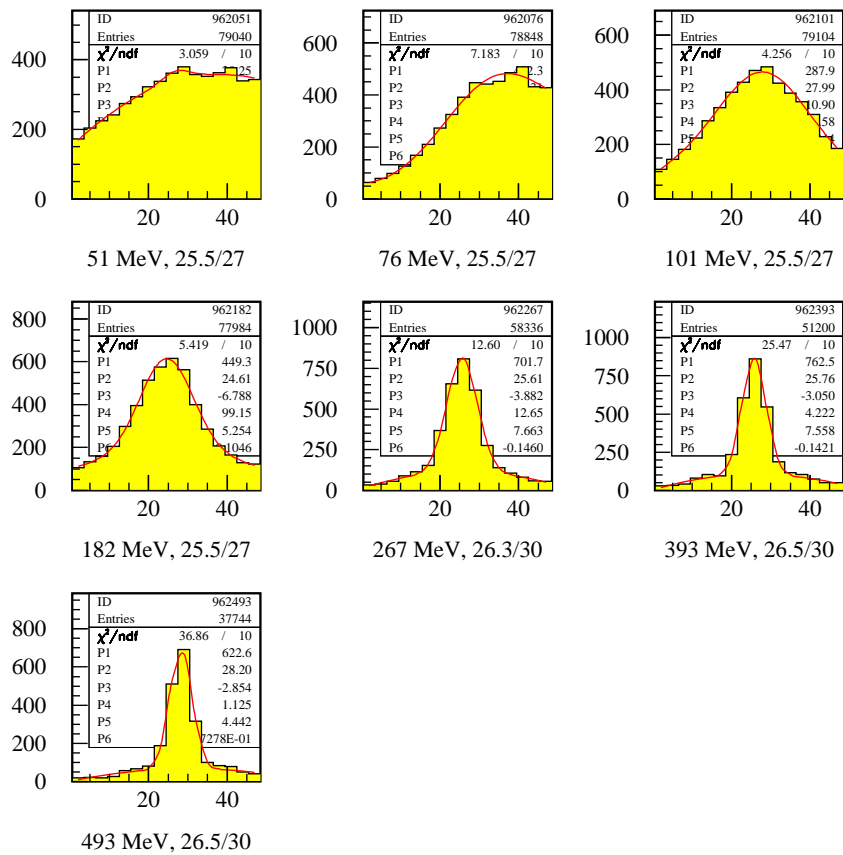


Figure 12: Charge-weighted profile for different BTF beam energies: the (horizontal) beam spot clearly increases at low energy due to the contribution of the multiple scattering (mainly due to the 1.5 mm thick aluminum window).

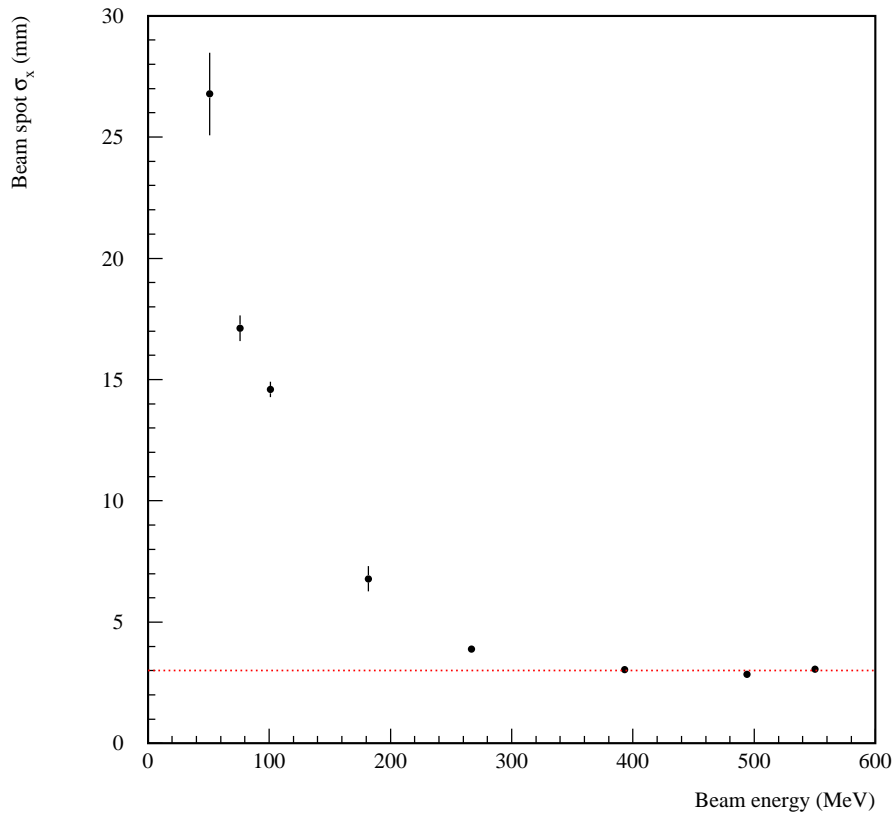


Figure 13: Horizontal beam spot size as a function of the beam energy: the behaviour is consistent with the $1/(\beta cp)$ dependance of the multiple scattering RMS angle at low energy, while approaches a constant value at higher energies, given by the contributions of the beam divergence and the fiber detector spatial resolution.

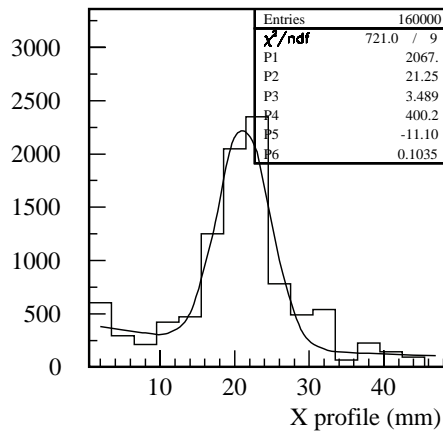
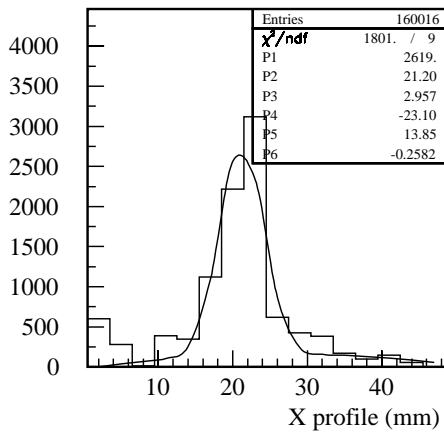
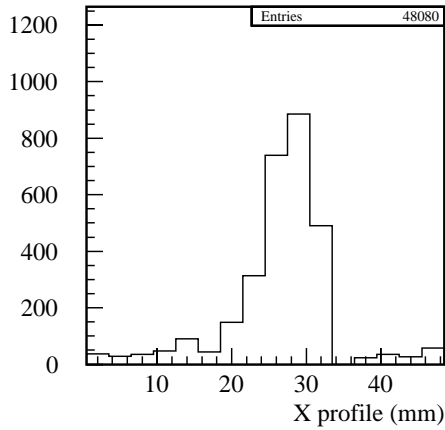


Figure 14: Horizontal beam spot size measured for different beam intensities and very similar beam focussing and collimation conditions: top, ≈ 2 particles/pulse; bottom left, ≈ 150 particles/pulse; bottom right, ≈ 600 particles/pulse.

4 Conclusions

The scintillating fiber detector has been built in order to have a simple, robust, easy to build and to manage beam spot monitor, capable of a millimetric resolution in a wide range of the BTF beam operating parameters (energy, intensity, focussing). The granularity of the readout has been sacrificed to the possibility of having as little as 32 ADC channels, so that they are all housed in a single 6U VME board, with only two 16-channels multianode photomultipliers, and to the possibility of having a good light yield even with only one electron crossing the fibers, with a relatively thin detector (only four layers per view).

However, the detector performed very well during the 2003 data taking, and allowed to continuously monitor the position and the size of the beam, with an accuracy of ≈ 2 mm, in both views.

Since a few seconds of data taking, at the maximum repetition rate of 49 pulses/s, are sufficient to get a satisfactory beam profile, the horizontal and vertical charge-weighted histogram have been integrated in the DAΦNE BTF control system. The shape of the beam in both x and y views can then be viewed online in the main panel of the BTF control system, as shown in Fig. 15. This demonstrated to be very useful tool, both in the beam optimization phases, and for driving the beam onto the users experimental apparatus with a good accuracy.

Most importantly, the detector is effective in a wide range of beam intensities, being efficient in single particle mode, and in the 10^3 particles/pulse range without any significant loss of resolution.

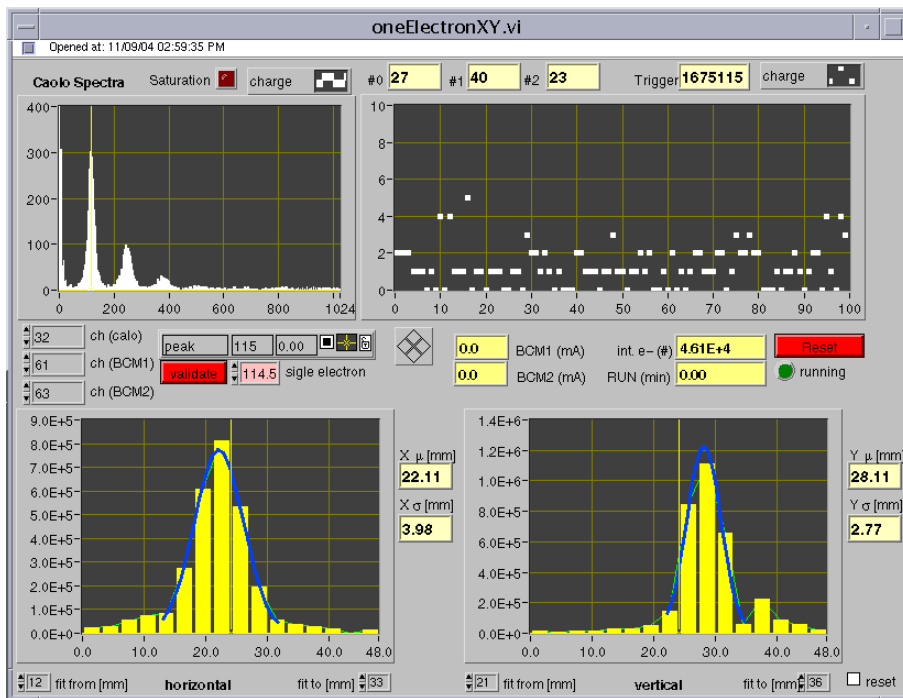


Figure 15: The horizontal and vertical beam profiles measured by means of the fiber detector have been integrated in the DAΦNE BTF control system, allowing an online monitoring of the position and size of the beam spot.

Acknowledgements

We thank U. Frasacco for the MAPMT cabling, G. Ferretti for the MAPMT mask construction, R. Clementi and R. Zarlenga for the scintillating fibers polishing, M. Sperati for the mechanical support.

We are grateful to S. Miscetti for the useful suggestions and for providing us the MAPMT.

We deeply thank P. Privitera and all the AIRFLY group for the precious collaboration during the data taking at the BTF.

Work partially supported by TARI contract HPRI-CT-1999-00088.

References

- [1] G. Mazzitelli and P. Valente, *Commissioning of the DAΦNE Beam Test Facility*, **LNF-03-003(P)** (2003).
- [2] G. Mazzitelli *et al.*, Nucl. Instrum. Meth. A **515** (2003) 516.
- [3] A. Antonelli *et al.*, Nucl. Instrum. Meth. A **370** (1996) 367.